

Structural analysis of clusters using configurational and orientational averaging in light scattering analysis

Norbert Riefler^a, Stefano di Stasio^b, Thomas Wriedt^{a,*}

^a*Stiftung Institut für Werkstofftechnik, Badgasteiner Strasse 3, 28359 Bremen, Germany*

^b*Istituto Motori C.N.R., Via Marconi 8, 80125 Napoli, Germany*

Abstract

We estimate the morphological parameters of soot particles in flames from static light scattering measurements. For these measurements established methods based on X-ray crystal structure analysis produce erroneous results. As an alternative method we investigate orientational and configurational averaging methods in light scattering analysis and compare their results with that from TEM analysis of collected clusters.

© 2004 Elsevier Ltd. All rights reserved.

Keywords: Static light scattering; Structural analysis; Orientational averaging; Configurational averaging

1. Introduction

Combustion of oil products is the worldwide dominant process for power generation. Optimization of combustion processes is therefore necessary to save energy as well as to reduce carbon dioxide and to avoid harmful waste products such as soot. Nevertheless soot is also a desired product, e.g. nano-size carbon black particles or high-tech soot have been used for tires as reinforcement for 100 years.

The aim of this work is the identification of the morphological structure from measured light scattering of soot clusters in flames. One other method is to collect soot cluster with a sample

*Corresponding author. Tel.: +49-421-218-2507; fax: +49-421-218-5378.

E-mail address: thw@iwt.uni-bremen.de (T. Wriedt).

holder. Then analysing the image of the cluster from an electron microscope provides the morphological parameters [1,2]. However this method is very slow and not suitable for process control. For in situ measurements it is convenient to use laser light scattering methods.

In the first section of this paper we will describe how to characterize fractal aggregates based on diffusion limited aggregation and how to estimate some essential parameters. Then we show some examples of a cluster–cluster aggregation algorithm which we developed. After a short reference to the established analysis we demonstrate the basics of the two averaging methods used for our structure analysis. The first is termed orientational averaging and the second is termed configurational averaging. The first method uses the calculated light scattering intensities of one cluster averaged over many different orientations. In the second method averaging is done after calculating light scattering intensities of many different clusters with arbitrary geometrical configurations. After that we describe the fitting procedure and the experimental setup which is used to get measured scattering intensities as the data base for the fits. In the following section we demonstrate the application of the averaging methods to the measurements and give at least an estimate of the described new method.

2. Cluster characterization

Aggregation of small particles yields aggregates characterized by their fractal dimension D_f and the so-called pre-factor k_f . These morphological parameters are related to the radius of gyration R_g and the radius of the primary spherules r_p in the form of a scaling law:

$$N = k_f \left(\frac{R_g}{r_p} \right)^{D_f} \quad (1)$$

with the radius of gyration determined from the position of each primary spherule \mathbf{r}_i to the geometrical center of the cluster $\mathbf{r}_0 = \sum_i \mathbf{r}_i / N$,

$$R_g^2 = \frac{1}{N} \sum_{i=1}^N (\mathbf{r}_i - \mathbf{r}_0)^2. \quad (2)$$

Eq. (1) is important because the values of parameters are linked to a real physical process. If $D_f \approx 1.8$ the process belongs to diffusion limited aggregation whereas $D_f \approx 2.1$ belongs to a reaction limited aggregation process.

The basis of the well established method for the characterization of clusters from measurements originates from solid state physics, especially from X-ray structure analysis. For an estimate of the fractal dimension one has to make many measurements in the backscattering region to be able to use statistical methods. In the case of our measurements the RDG-theory is not able to fit successfully the whole angular pattern of measurements, in particular, the features of the experimental data at backscattering angles.

In this paper we use orientational as well as configurational averaging to identify the morphological parameters of the clusters. Both methods are used in other fields, e.g. calculation of the orientational average of spin amplitudes coming from NMR signals [3] or in mechanics of solids [4]. Configurational average is also used in crystallography to calculate the electronic

interaction, e.g. in X-ray absorption experiments [5] or in alloy research [6,7]. Kouzakov et al. [7] calculates the configurational average of the differential cross sections.

3. Cluster–cluster aggregation

Based on an algorithm described by Filippov et al. [8] we have developed a fast Fortran program to generate clusters as input data for light scattering programs. For our investigations we generated a data base consisting of clusters with nine different values of the fractal dimensions ($D_f = 1.2, 1.3, \dots, 2.0$), eight different numbers of primary spherules ($N_p = 60, 70, \dots, 130$) and seven different radii of primary spherules ($r_p = 5, 7.5, 10, 15, 20, 25, 30$ nm). For each of these morphological parameters we generated 300 different clusters and computed the corresponding scattering diagrams under one orientation. Besides that we also generated three clusters for each morphological parameter set and calculated their orientational averaged scattering quantities.

For examination of the convergence of the averaging methods we also created separate simulation series. Examples of two clusters under two different perspectives are shown in Figs. 1 and 2. The clusters have the same morphological parameters: $D_f = 1.8$, $N_p = 110$, $r_p = 15$ nm and $k_f = 1.5$. The resulting radius of gyration is for both clusters $R_g = 0.163$ μm and their geometrical radius of a surrounding sphere is $R_0 = 0.2503$ and 0.2498 μm for cluster 1 and cluster 2, respectively.

We also examine our cluster–cluster generation program regarding the correctness of the preset morphological parameters D_f , N_p , k_f and r_p . The geometrical data of a cluster consists of the radius of primary particles r_p , each spatial position of them and of course their number N_p . This data determine the radius of gyration R_g using Eq. (2). So the only unknown parameter of the scaling law (Eq. (1)) are D_f and k_f . With a method described by Bushell and Amal [9] we calculate the distance distribution function $c(r)$ of big clusters with at least $N_p = 500$ primary particles. The slope of $c(r)$ in the range of $5r_p < r \ll R$ corresponds with the fractal dimension D_f . Smaller clusters show too much oscillations so it is in practice impossible to fit a straight line on the curve of $c(r)$. However the big clusters shows very good agreement with the preset fractal dimension D_f .

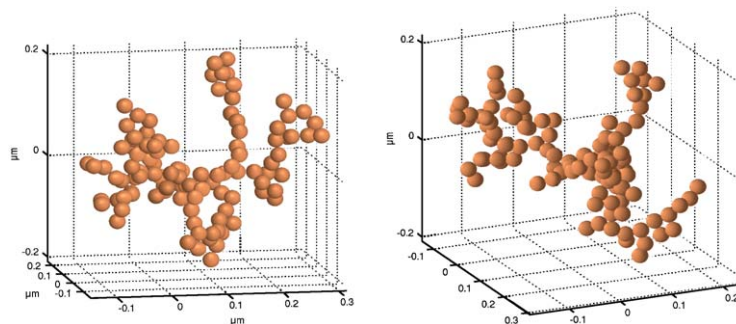


Fig. 1. Cluster 1 under an azimuthal and an elevation angle of 66° and 20° (left) and -10° and 10° (right).

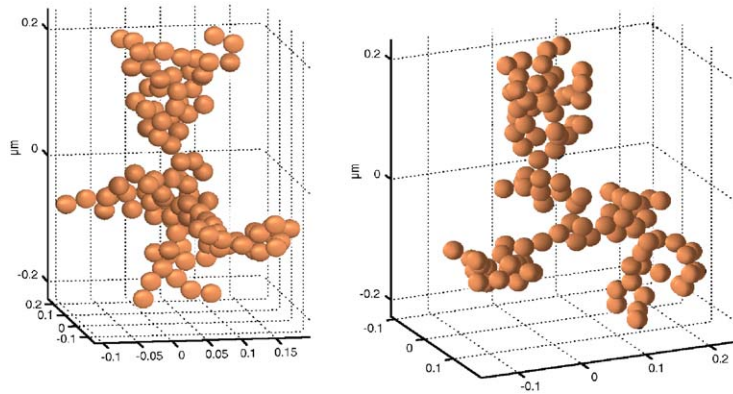


Fig. 2. Cluster 2 under the same two viewpoints as in Fig. 1.

4. Light scattering simulation

A program based on the T-matrix method [10] was used to calculate the T-matrix of the clusters. This method produces exact light scattering quantities and it is energetically conservative, in opposite of e.g. the Rayleigh–Debye–Gans approximation used in the conventional structure analysis described below.

With the T-matrices we calculate the single as well as the orientational averaged light scattering quantities. All diagrams shown in this paper are vertical polarized intensities as response to vertical polarized incident beam.

The intensity $I(\theta)$ corresponds with the differential scattering cross section (DSCS) $dC_{\text{sca}}/d\Omega$ [11,12]:

$$C_{\text{sca}} = \int_0^{2\pi} \int_0^\pi \frac{dC_{\text{sca}}}{d\Omega} \sin(\theta) d\theta d\phi = \frac{1}{I_{\text{inc}}} \int_{4\pi} I(\vec{n}_{\text{sca}}) d\vec{n}_{\text{sca}} \quad (3)$$

with the total scattering cross section C_{sca} , the solid angle $d\Omega$, the azimuthal angle ϕ which define the scattering plane, the scattering angle θ , the incident radiation intensity I_{inc} and the unit vector of scattering $\vec{n}_{\text{sca}} = \vec{r}/r$.

For $\phi = 0$ and in a spherical coordinate system the unit vector \vec{n}_{sca} corresponds to the scattering angle θ and thus $I(\vec{n}_{\text{sca}}) = I(\theta)$.

5. Analysis methods

5.1. Conventional structure analysis

A method to estimate all parameters of the scaling law for cluster aggregates are described by Oh and Sorenesen [13], Megaridis and Dobbins [14,15], Samson et al. [16] and other authors. Here we only want to sketch the basics of this methods.

In the power law regime the fractal dimension is related to the vertical–vertical polarized intensity I_{vv} :

$$I_{vv} \sim q^{-D_f}, q^2 R_g^2 \gg 1. \tag{4}$$

So a log–log plot of the vertical–vertical polarized intensity I_{vv} versus high values of the scattering vector q gives the fractal dimension:

$$\frac{\log(I_{vv})}{\log(q)} \sim -D_f. \tag{5}$$

In the Guinier regime where $q^2 R_g^2 \ll 1$ the radius of gyration is related with the intensity I_{vv} :

$$\frac{I_{vv}(q)}{I_{vv}(0)} = \exp(-q^2 R_g^2/3). \tag{6}$$

An approximation of the exponential gives:

$$\frac{I_{vv}(0)}{I_{vv}(\theta)} = 1 + q^2 R_g^2/3 \tag{7}$$

and a graphical plot of the intensity against the squared scattering vector gives the radius of gyration R_g .

Based on measuring the turbidity and the extinction cross sections Sorensen et al. [17] described a graphical network-analysis scheme to evaluate the number and the radius of primary particles N and r_p .

5.2. Orientational averaging

No particle comes alone in a measurement setup. In the case of simulating light scattering measurements, one has to average the physical quantities in the measuring volume. Usually this will be done for one cluster. The principal equation for orientational averaging is a triple integral over the three Euler angles [3,4]:

$$\langle I(\theta) \rangle = \int_0^{2\pi} \int_0^\pi \int_0^{2\pi} I(\theta; \alpha, \beta, \gamma) \sin(\beta) \, d\alpha \, d\beta \, d\gamma. \tag{8}$$

This equation is sometimes called “ensemble averaging” [12].

There are different methods to get orientational averaged results. In one method the averaged values is calculated analytically over continuous particle orientations [18,19]. In the other method results are integrated over discrete orientations [20]. A comparison of both methods is given by Xu et al. [21].

In this paper we use the discrete method. The orientation of the cluster will be changed in equally sized steps of $N_\alpha, N_\beta, N_\gamma$ for each of the three Euler angles α, β, γ [20],

$$\langle I(\theta) \rangle = \sum_{n_\alpha=1}^{N_\alpha} \sum_{n_\beta=1}^{N_\beta} \sum_{n_\gamma=1}^{N_\gamma} I(\theta; \alpha, \beta, \gamma) \sin\left(\frac{n_\beta 2\pi}{N_\beta}\right) \frac{n_\alpha 2\pi}{N_\alpha} \frac{n_\beta \pi}{N_\beta} \frac{n_\gamma 2\pi}{N_\gamma}, \tag{9}$$

where $I(\theta)$ is the intensity at the scattering angle θ . Instead of $I(\theta)$ each other scattering quantity can be averaged like the Mueller matrix elements.

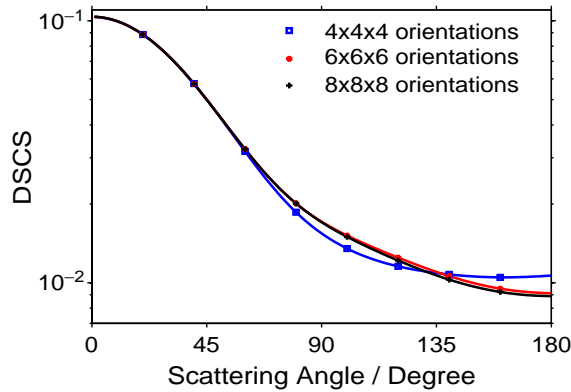


Fig. 3. Convergence of the orientational averaged vv scattering diagrams.

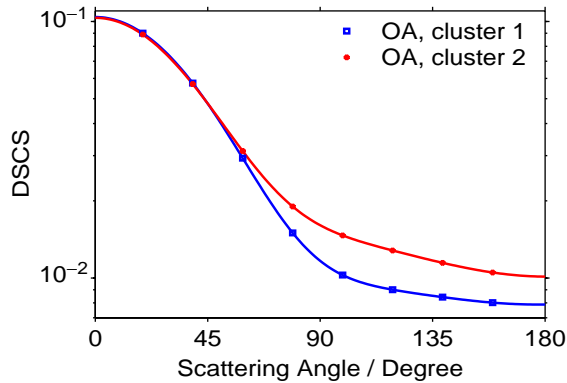


Fig. 4. Discrepancy of the scattering diagrams of the two orientational averaged cluster of Fig. 1.

Usually the number of different orientations needed for convergence of the average is within the range of 300 to 1000 for complex aggregates. As an example Fig. 3 shows the differential scattering cross sections (DSCS) of three orientational averaging runs with 64, 216 and 512 different orientations for one cluster. In our case $N_\alpha = N_\beta = N_\gamma = 8$ are sufficient for convergence of the scattering diagrams even for clusters with small fractal dimension of $D_f = 1.2$. Such clusters are long and narrow and orientational averaging would need more different orientations than in the case of clusters with $D_f = 1.8$ which are more symmetric. Altogether in our light scattering simulations we always averaged over 512 different orientations.

Fig. 4 shows a remarkable fact. Even after orientational averaging the two clusters from Figs. 1 and 2 give different scattering diagrams although they have the same morphological parameters. Increasing the number of orientations did not change this result. Such a variation was also seen experimentally by Lu et al. [22] and by Seeley et al. [23].

As a consequence for our averaging method we take into account the orientational averaged results of three different clusters with the same morphological parameters.

5.3. Configurational averaging

The other method for identification of morphological parameter uses different clusters with arbitrary spatial geometry but with the same morphological parameters. To our knowledge there are only a few references concerned with configurational averaging of scattering quantities. Farias et al. [24] compared the smoothing of scattering patterns due to orientational averaging of one cluster under 128 orientations and configurational averaging of 128 different clusters with the same morphological parameters. The orientational averaged scattering diagrams show more oscillations than the configurational averaged. But if one increase the number of orientations these oscillations will vanish, as we demonstrated in Fig. 3.

Saltiel et al. [25] used a database of agglomerates to match measured scattering matrix results to results obtained from theoretical calculations. However they did not describe how they performed their matching procedure.

To get an averaged light scattering quantity of N_{cl} different cluster configurations, we add up the wanted physical quantity in a simple manner:

$$\langle I(\theta) \rangle = \frac{1}{N_{cl}} \sum_{n=1}^{N_{cl}} I_n(\theta) \tag{10}$$

with the intensity $I_n(\theta)$ at the scattering angle θ for the n th cluster.

In our case of using a database of aggregates and scattering quantities of different morphological parameters it is necessary to ensure the uniqueness of the cluster for configurational averaging. Therefore a control routine was implemented in the fit algorithm to avoid repeated use of one and the same cluster.

Convergence of the computed DSCS is reached for more than 300 different clusters, see Fig. 5. For testing the reproducibility of our method we generated two independent data sets. Each set consists of 1000 different clusters with the same parameters $D_f = 1.8$, $N = 110$, $k_f = 1.5$ and $r_p = 15$ nm together with their corresponding scattering diagrams. They show identical behaviour for a high number of clusters included for averaging in Fig. 6. However the result for another run

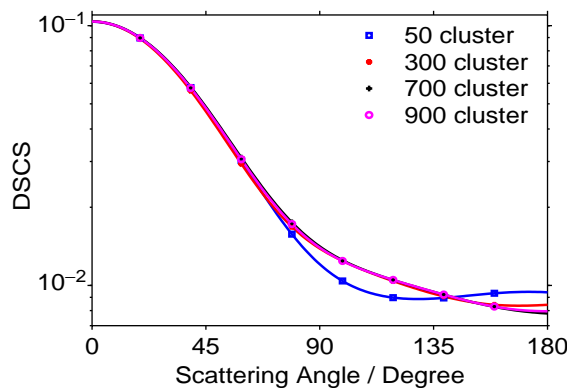


Fig. 5. Convergence of the configurational averaged vv scattering diagrams.

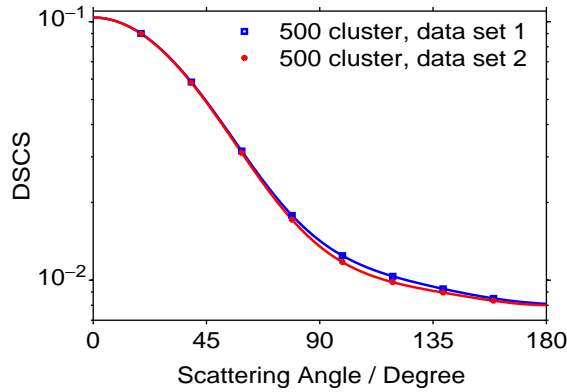


Fig. 6. Convergence of different data sets for 500 clusters.

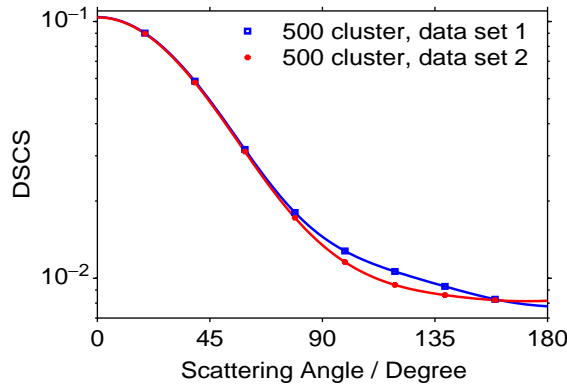


Fig. 7. Convergence of different data sets for another averaging run for 500 clusters.

of the averaging procedure shows some minor discrepancies (Fig. 7). The reason for this might be the arbitrary choice of clusters in the averaging procedure. Another run of the procedure uses altogether more different clusters than in a previous run and so there are two different averaging results.

Fig. 8 shows a comparison between configurational and orientational averaging, again with the morphological parameter like before. The diagrams of the orientational averaging are one and the same like those of Fig. 4. They show more discrepancies than the configurational averaged diagrams. However all results lie within the same region.

5.4. Fitting procedure

To find the morphological parameter of the aggregates in a flame we fitted the measured intensities using a least squares method. Therefore the angle resolved simulated scattered intensities had to be scaled. We use two scaling methods. The first method takes the measured

intensity at one angle, for example at $I_{\text{meas}}(90^\circ)$, and calculates the scaling factor of the simulated scattering diagram at this angle with the corresponding simulated intensity I_{sim} , $s_{\text{fix}} = I_{\text{sim}}(90^\circ)/I_{\text{meas}}(90^\circ)$. All other simulated intensities will be multiplied by s_{fix} .

The other method scales the complete simulated scattering diagram as smooth as possible to the measured diagram over the observed angles θ :

$$s_{\text{smooth}} = \sum_{\theta} I_{\text{sim}}(\theta) / \sum_{\theta} I_{\text{meas}}(\theta). \tag{11}$$

In the experiment the detector will have a certain aperture. Therefore we implemented a detector integration. The routine integrates the simulated light scattering intensities over a specified range of angles correspondingly to the detector aperture for each scattering angle measured in the experiments.

The fitting procedure is a least square method. The sum of the squared differences between measured and simulated intensities gives a measure of the quality of the simulated scattering diagram. The differences are calculated logarithmically over a specific scattering range i of measured intensities:

$$\Delta = \sum_i (\log_{10}(I_m) - \log_{10}(I_s))^2. \tag{12}$$

Generally the logarithm gives better results than using pure intensities because of the great range of different intensities.

Because the averaged results vary for different clusters with exactly the same morphological parameter (see Fig. 8), it is necessary to run the averaging procedure more than once. In the case of orientational averaging we created three clusters for each morphology and calculated the orientational averaged scattering quantities. In the case of configurational averaging we introduced the number of combinations N_{comb} . The procedure of taking N_{cl} different clusters from the data base and average their scattering quantities will be repeated for N_{comb} times. Without this the probability of getting a wrong result for the correct morphology is high especially for small values of N_{cl} . So repeated averaging makes the result more stable. The morphological parameter for the best fit should at least correspond with that of the real measured aggregate.

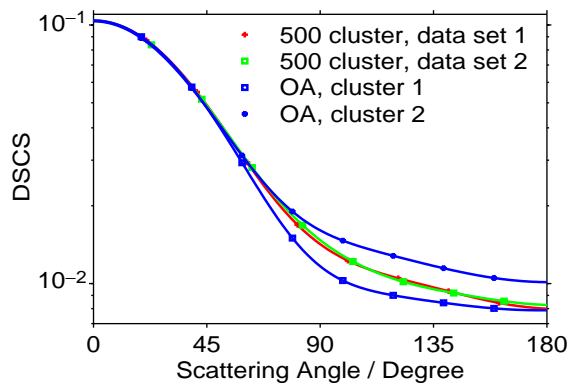


Fig. 8. Comparison between configurational and orientational averaged vv scattering diagrams.

6. Experiments

The experiments are fully described in details in previous work [26–28]. In the following only a short description will be given.

Soot aggregates are produced in air atmosphere by a Bunsen burner of 10 mm inner diameter, burning ethylene (purity better than 99%). The properties of the gas at the burner exit are represented by a Reynolds number of about 110–170, which corresponds to efflux velocities of 9.1–14.5 cm/s. The light source is a vertically polarized argon-ion laser tuned on the line at 514.5 nm. The laser beam is mechanically chopped at 931 Hz. The burner is fixed on a goniometer, which allows determination of the scattering angles θ . A scheme of the detection system is reported in Fig. 9. A measurement volume $MV \approx 40 \times 10^{-6} \text{ mm}^3$ at 90° , corresponding to a detection angle $DA = 6.38^\circ$, is located at the center of the flame on the flame axis at different heights above the burner. The ethylene–air diffusion flame has cylindrical symmetry and both the soot volume fraction and primary size have an inhomogeneous radial profile. Nevertheless, all the measurements are taken at radial coordinate zero, namely on the flame axis. At different height-above-burner (HABs) we expect, apart from morphological variations of aggregate shape and size variation of primary particles, also some variations of refractive index, owing to the continuous dehydrogenation process occurring within the flame. In any event, the conventional analysis for inferring fractal dimension and radius of gyration is poorly depending on the possible variations of soot optical properties due to the scarce variations with respect to the refractive index of the scattering angular pattern functions $F(\theta)$ for vertical–vertical light $I_{VV} = N_p I_{VV,R} F(\theta)$ scattered by aggregates of Rayleigh primary particles, $I_{VV,R}$ is the vertical–vertical light intensity scattered by a single isolated primary particles [29,30].

The measurement volume (MV) is determined in the experiments by the intersection of the laser beam and the optical detection cone, which collects light scattered by the particles inside MV

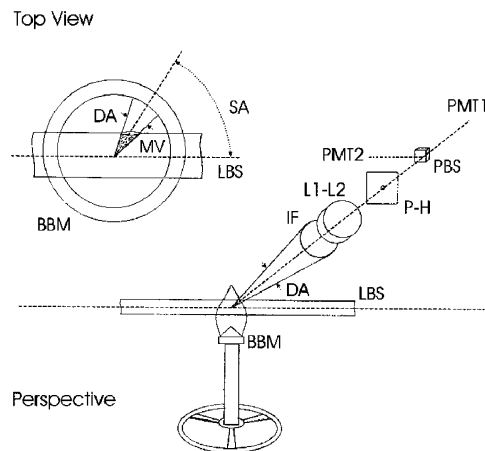


Fig. 9. Experimental setup. LBS = Laser Beam Section; DA = Detection Angle; L1 = collecting Lens (diameter 25.4 mm; focal length 300 mm); L2 = focusing Lens (diameter 25.4 mm; focal length 50 mm); IF = Interference Filter; P-H = Pin-Hole (1mm dia); PBS = Polarizing Beam Splitter; PMT1, PMT2 = Photo-Multiplier Tubes; SA = scattering angle θ ; MV = Measurement Volume; BBM = Bunsen Burner Mouth.

(Fig. 9, top). Thus, the measurement volume result reaches its minimum MV_{90° at 90° scattering angle (SA). Several thousands of clusters are located within the MV at $\theta = 90^\circ$ depending on HAB. For instance at $HAB = 16$ mm we estimate from scattering and separate extinction measurements that about 2000 clusters lie inside MV. At scattering angles θ different from 90° the measuring results will vary according to the geometry factor $1/\sin(\theta)$. After emerging out of the flame, the scattered light is collected by an optical detection system (Fig. 9, bottom), which is composed by two lenses (focal length 300 mm and 50 mm), an interference filter (FWHM 1 nm), a pinhole (1 mm), a polarizing beam splitter, and two photomultiplier tubes (PMT). Measurements of vertical–vertical light intensities I_{vv} , are performed. A lock-in amplifier is used to discriminate light-scattering signals against flame luminosity and out-of-band noise.

Measurements at scattering angles θ between 10° and 160° are taken. This corresponds, for $\lambda = 514.5$ nm, to scattering wave vector moduli $q \equiv (4\pi/\lambda)\sin(\theta/2)$ within the range $2.0 \mu\text{m}^{-1} \leq q \leq 24 \mu\text{m}^{-1}$. The signal at the output of the lock-in amplifier is then multiplied by $\sin(\theta)$ to account for variation of the volume focused by the optical system when θ is changed. Scattering measurements are then corrected to account for the extinction (about 1%) undergone by the laser beam in passing through the flame.

7. Results and discussion

First we want to show results from the conventional structure analysis applied to our measurements. Figs. 10 and 11 shows the graphical evaluation of the fractal dimension D_f and the radius of gyration R_g for measured intensity at $HAB = 16$ mm and Figs. 12 and 13 for $HAB = 30$ mm, respectively.

On experimental basis the scattering patterns are measured, from which the D_f and R_g are obtained. Moreover, the N_p and r_p are inferred again from the experimental data relative to the dissymmetry ratio $R_{vv}(20/90) = I_{vv}(20^\circ)/I_{vv}(90^\circ)$ and from the SEM measurements, respectively, along a trial-and-error procedure described elsewhere [31,32]. It was also demonstrated with

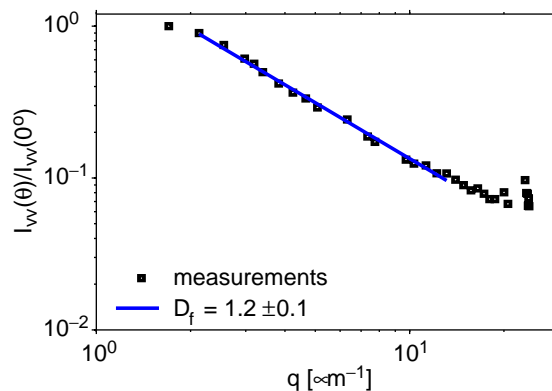
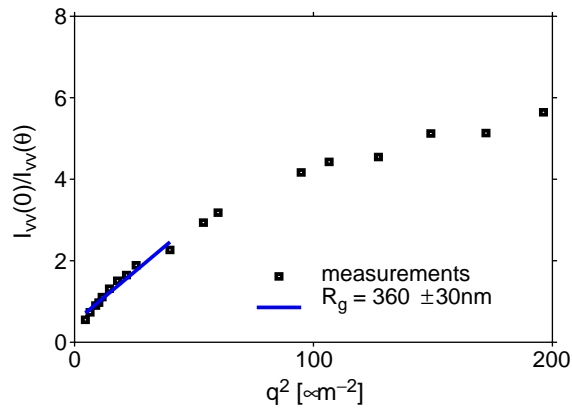
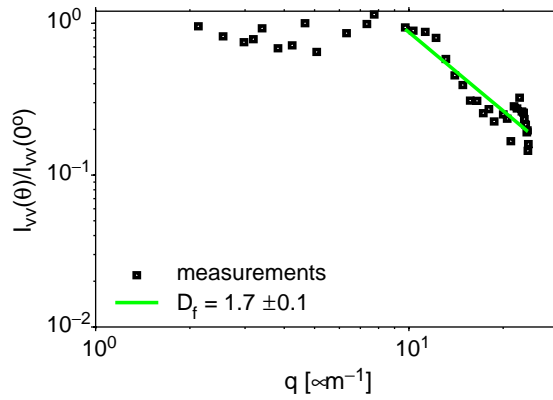
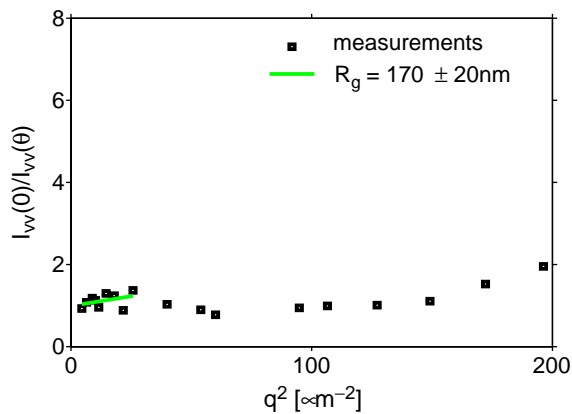


Fig. 10. Estimation of the fractal dimension D_f for $HAB = 16$ mm.

Fig. 11. Estimation of the radius of gyration R_g for HAB = 16 mm.Fig. 12. Estimation of the fractal dimension D_f for HAB = 30 mm.Fig. 13. Estimation of the radius of gyration R_g for HAB = 30 mm.

previous work that the dissymmetry ratios are poorly sensitive to the refractive index variations thus being very attractive diagnostic tools [30].

The conventional structure analysis does not require any a priori knowledge of the soot properties, including the soot refractive index and present all the advantages to employ only scattering measurements.

For examining the applicability of the orientational and the configurational averaging method we begin with no a priori information about the morphology of the measured soot aggregates except the refractive index of soot $n = 1.57 + i0.56$ [33], a standard value which do not correspond to the work of Dalzell and Sarofim [34]. They proposed a value of $n = 1.57 + i0.46$ at $\lambda = 550$ nm.

The other presumed value is $k_f = 1.5$ for the fractal prefactor in Eq. (1) [35]. This value is not identical with that reported in the cited literature, but it is very similar. Our detector integration routine integrates the simulated light scattering intensities from $-3^\circ, \dots, +3^\circ$ around each measured intensity.

In the fitting procedure the parameter variation runs over nine values of different fractal dimensions D_f , eight different numbers of primary spherules N_p and seven different radii of primary spherules r_p , so altogether a fit over the complete data base uses 504 different morphologies. In the case of orientational averaging, there are three different clusters for each combination of the 504 morphologies. We tried to fit the measurements of angular scattering pattern and the r_p from SEM reported in previous work [27,28] with our simulations which takes into account the configurational averaging. The starting D_f and N_p in our simulations will be taken from the values inferred by the trial-and-error procedure, described in [28], to match measurements of scattered intensities in the Guinier and power law regimes and the measured dissymmetry ratio $R_{vv}(20^\circ/90^\circ)$.

The “bump” in the scattering pattern near $\theta = 135^\circ$ (see Fig.14) is due to the transition between the fractal power law $I(q) \sim qD_f$ and the Porod power law $I(q) \sim q^{-4}$. Unfortunately, the Porod’s law is valid for primary units which are perfectly spherical, homogeneous and with smooth surface. This is not the case for soot primary particles. In particular, the higher the HAB the more they are carved. This corresponds to the fact that oxidation proceeds towards the interior through pores. This irregularity on the surface will be reflected in so-called “interference effects” which are due to the interference between the scattering by the main structure unit (primary spherule) and the characteristic size of the irregularities at their surface.

A fit over the complete data base delivers good agreement with the SEM analysis for the fractal dimension D_f , see Fig. 14 for the measurement at height of the burner HAB = 16 mm and Fig. 15 at HAB = 30 mm. However, the results for the numbers of primary spherules N_p and radius of primary spherules r_p seems to be wrong compared to SEM analysis.

A better result for HAB = 30 mm follows after narrowing the evaluated measurement range of the scattering angles to values between 47° and 146° , see Fig. 16. However, further narrowing to the smaller range between 55° and 125° , the results get worse, see Fig. 17. The result and fits using other ranges of θ indicates that there is no typical scattering range like the Guinier regime which have to be used to estimate e.g. the fractal dimension.

For a HAB = 16 mm there is a similar trend for getting results with higher fractal dimension as well as higher number of primary spherules and primary particle radius after narrowing the measurement range.

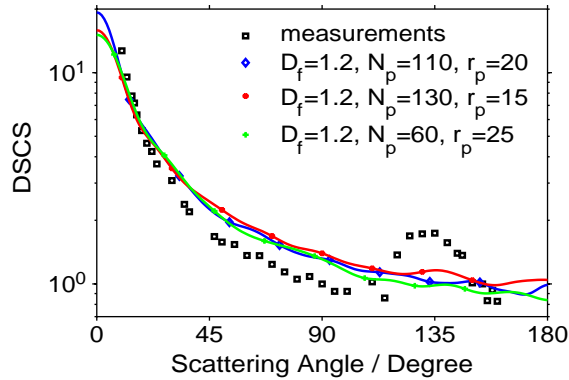


Fig. 14. Orientational averaging fit for HAB = 16 mm.

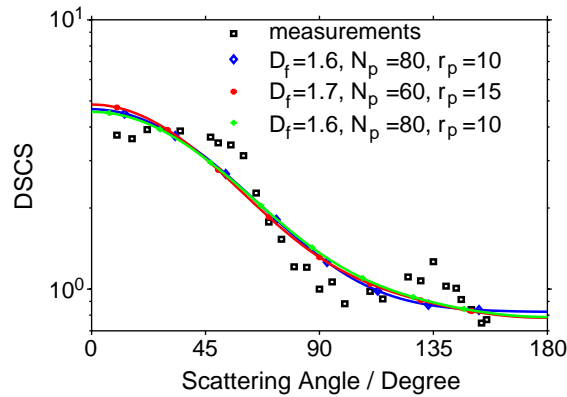


Fig. 15. Orientational averaging fit for HAB = 30 mm.

In the case of configurational averaging there are more parameters which have to be varied. Besides D_f , N_p and r_p another important parameter is the number of clusters N_{cl} from Eq. (10).

First we consider the measurements with HAB = 16 mm. The best fit for the fractal dimension does not corresponds as well as that from the orientational averaging, see Fig. 18. Narrowing the data range for the fit to a scattering range of 10° – 100° , the result for the fractal dimension agrees with that from SEM analysis, see Fig. 19. However the number and the radius of the primary particles fits worse.

In the case of measurements with HAB = 30 mm, (Fig. 20) the result for the fractal dimension $D_f = 1.7$ agrees with the value obtained in previous experimental work [27], see Fig. 18. However, we did not get very good results for N_p and r_p from a fit using the complete data base. After narrowing the data range for the fit, the result for the fractal dimension is smaller than the expected $D_f = 1.7$, but the values of N_p and r_p agrees better with that from SEM analysis, see Fig. 21. Narrowing to a small range around $\theta = 90^\circ$ gives very good agreement for these parameters, see Fig. 22.

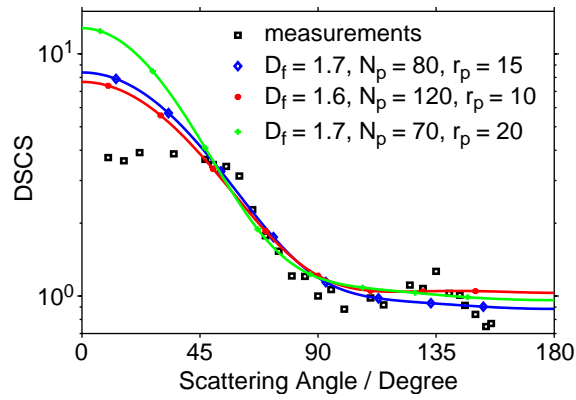


Fig. 16. Orientational averaging fit for HAB = 30 mm for scattering range of 47°–146°.

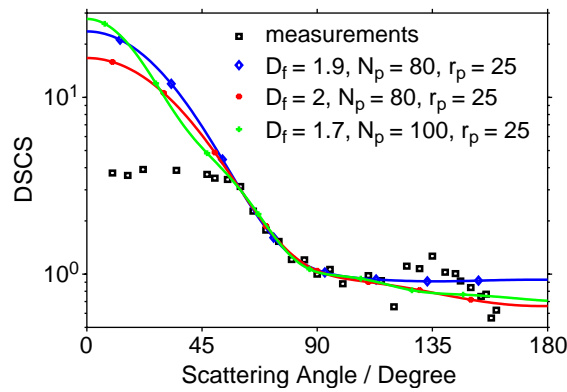


Fig. 17. Orientational averaging fit for HAB = 30 mm for scattering range of 60°–115°.

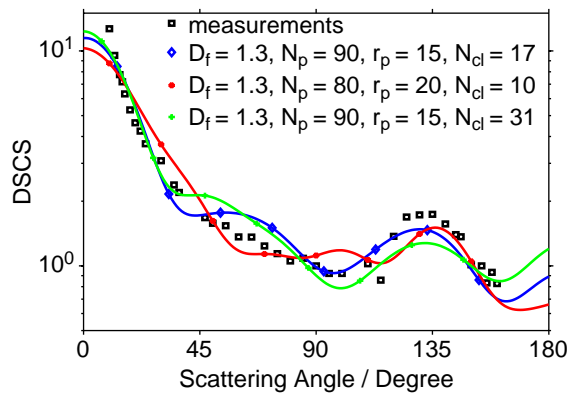


Fig. 18. Configurational averaging fit for HAB = 16 mm over the complete data range.

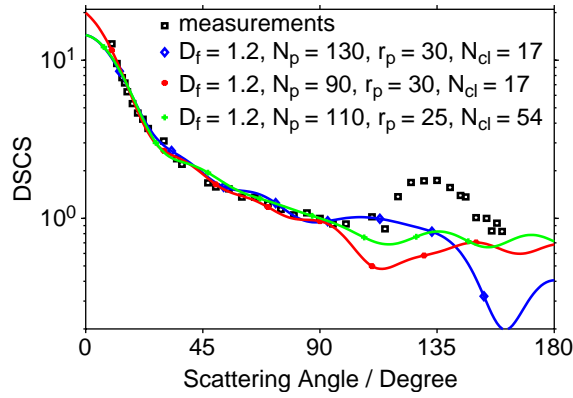


Fig. 19. Configurational averaging fit for HAB = 16 mm for a scattering range of 10°–100°.

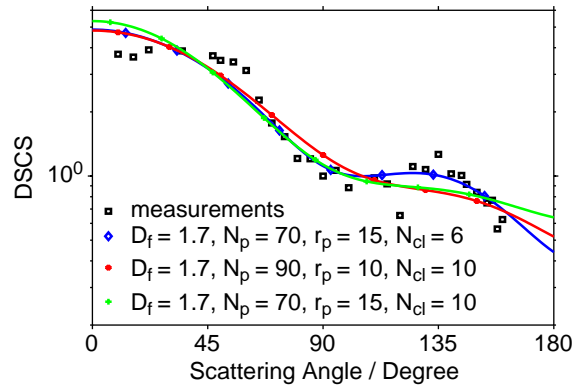


Fig. 20. Configurational averaging fit for HAB = 30 mm over the complete data range.

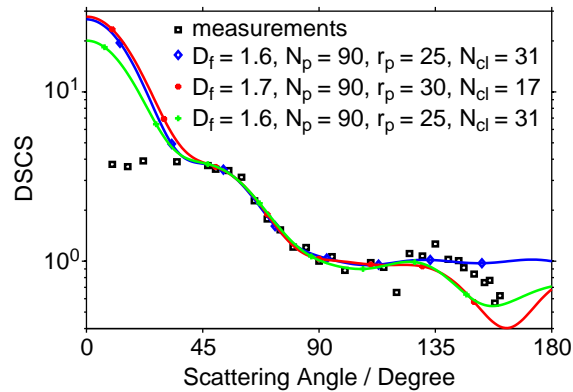


Fig. 21. Configurational averaging fit for HAB = 30 mm for scattering range of 47°–115°.

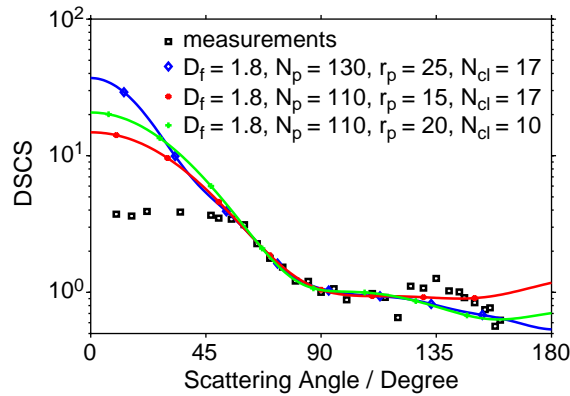


Fig. 22. Configurational averaging fit for HAB = 30 mm for scattering range of 60°–115°.

Table 1
Composition of the results for HAB = 16 mm

Method	HAB = 16 mm		
	D_f	N_p	r_p
LS + SEM	1.2±0.1	60±10	15±3 nm
OA, Fig. 14, best fit	1.2	70	25 nm
OA, Fig. 14, average	1.2	107	18 nm
CA, Fig. 18, best fit	1.3	90	15 nm
CA, Fig. 18, average	1.3	87	17 nm
CA, Fig. 19, best fit	1.2	130	30 nm
CA, Fig. 19, average	1.2	110	28 nm

In all results of configurational averaging the number of clusters N_{cl} is much smaller than the number of real cluster of about 5000 and more in the measuring volume (see p. 11). This difference may be explained by the fact that the cluster moves in the flame whereas in the simulation the light scattering response is static. Another difference is that in the measurement volume the morphological parameter of the soot particles are distributed whereas the simulations are based on one specific parameter set.

At any rate the light scattering measurement will be represented through the light scattering of N_{cl} clusters.

In Table 1 we summarized the values of the SEM analysis together with the results of the orientational averaging (OA) and the configurational averaging (CA). We insert the best fit and the average of the three best fitting results of each of the previous figures (Table 2). In both tables the bold typed values agree with the SEM analysis. Altogether the CA seems to produce better results.

With the averaged values from Fig. 18 we get a radius of gyration of $R_g = 350$ nm if we use the geometrical data of our clusters in the data base all having the parameters $D_f = 1.3$, $N_p = 90$ and

Table 2

Composition of the results for HAB = 30 mm

Method	HAB = 30 mm		
	D_f	N_p	r_p
LS + SEM	1.7±0.1	110±15	20±4 nm
OA, Fig. 15, best fit	1.6	80	10 nm
OA, Fig. 15, average	1.6	73	12 nm
OA, Fig. 16, best fit	1.7	80	15 nm
OA, Fig. 16, average	1.7	90	15 nm
OA, Fig. 17, best fit	1.9	80	25 nm
OA, Fig. 17, average	1.9	87	25 nm
CA, Fig. 20, best fit	1.7	70	15 nm
CA, Fig. 20, average	1.7	77	13 nm
CA, Fig. 21, best fit	1.6	90	25 nm
CA, Fig. 21, average	1.6	90	27 nm
CA, Fig. 22, best fit	1.8	130	25 nm
CA, Fig. 22, average	1.8	117	20 nm

$r_p = 15$ nm. For $D_f = 1.8$, $N_p = 120$ and $r_p = 20$ nm corresponding to the averaged results of Fig. 22 we get a radius of gyration of $R_g = 0.227$ nm. Both values of R_g are higher compared with Fig. 11 and Fig. 13, but the tendency is the same.

8. Conclusion

We intended to test a new method for analysing the structure of soot cluster. The combination of orientational and configurational averaging seems to be a promising method for evaluation of morphological parameters from aggregates with laser light scattering measurements. Especially configurational averaging fits the simulated scattering quantities very smooth to the measured. The reason for this is that this method is able to use arbitrary numbers of clusters in contrast to orientational averaging. Although one can average over less different orientations in an orientational averaging, this has the disadvantage of how to interpret the result. However using e.g. 17 different clusters for a configurational averaging have a unique meaning, namely that there are 17 clusters necessary for the best fit (see Fig. 20). And these 17 clusters represents the corresponding measurement.

Another advantage is that the method described in this paper uses the T-matrix method to compute the light scattering quantities. This method is energetically conservative and it produces exact values, especially in the backscattering region where the RDG-approximation fails.

The method outlined here is a little bit cumbersome because of the need of a previously build data base. A more flexible computing tool seems to be desirable. Especially the fractal prefactor k_f and the refractive index n were not varied because this would blow up the size of the data base. A fitting procedure which does not use a data base could be more suitable to fit measured data.

References

- [1] Dobbins RA, Megaridis CM. Morphology of flame-generated soot as determined by thermophoretic sampling. *Langmuir* 1987;3:254–9.
- [2] Cai J, Lu N, Sorensen CM. Comparison and morphology of soot aggregates as determined by light scattering and electron microscope analysis. *Langmuir* 1993;9:2861–7.
- [3] Edèn M, Levitt MH. Computation of orientational averages in solid-state nmr by gaussian spherical quadrature. *J Magn Reson* 1998;132:220–39.
- [4] Tamuzh VP, Lagzdins AZ, Teters G, Kregers A. *Orientalional averaging in mechanics of solids*. Essex: Longman Scientific and Technical; 1992.
- [5] Loeffen PW, Pettifer RF. Thermal dependence of multiple scattering using independently established dynamical information. *Physica B* 1995;39–41:39–41.
- [6] Habar M, Stauffer L, Wille LT, Dreyse H. Theoretical study of the first stages of ni adsorption on pt(1 1 1). *Surf Sci* 2003;532–535:53–7.
- [7] Kouzakov KA, Berakdar J. Emission of correlated electrons from random alloys. *J Phys: Condens Matter* 2003;15:L41–7.
- [8] Filippov AV, Zurita M, Rosner DE. Fractal-like aggregates: relation between morphology and physical properties. *J Colloid Interface Sci* 2000;229:261–73.
- [9] Bushell G, Amal R. Fractal aggregates of polydisperse particles. *J Colloid Interface Sci* 1998;205:459–69.
- [10] Doicu A, Wriedt T. T-matrix method for electromagnetic scattering from scatterers with complex structure. *JQSRT* 2001;70:663–73.
- [11] Bohren C, Huffman D. *Absorption and scattering of light by small particles*. New York: Wiley; 1983.
- [12] Mishchenko M, Hovenier J, Travis L. *Light scattering by nonspherical particles*. San Diego: Academic Press; 2000.
- [13] Oh C, Sorensen CM. Light scattering study of fractal cluster aggregation near the free molecular regime. *J Aerosol Sci* 1997;28:937–57.
- [14] Megaridis CM, Dobbins RA. Morphological description of flame-generated materials. *Combust Sci Technol* 1990;71:95–109.
- [15] Dobbins RA, Megaridis CM. Absorption and scattering of light by polydisperse aggregates. *Appl Opt* 1991;30:4747–54.
- [16] Samson RJ, Mullholand GW, Gentry JW. Structural analysis of soot agglomerates. *Langmuir* 1987;3:272–81.
- [17] Sorensen CM, Cai J, Lu N. Light-scattering measurements of monomer size, monomers per aggregate and fractal dimension for soot aggregates in flames. *Appl Opt* 1992;31:6547–57.
- [18] Khlebtsov NG. Orientalional averaging of light-scattering observables in the t matrix approach. *Appl Opt* 1992;91:5359–65.
- [19] Mackowski DW, Mishchenko MI. Calculation of the t matrix and the scattering matrix for ensembles of spheres. *J Opt Soc Am A* 1996;13:2266–78.
- [20] Shu G, Charalampopoulos TT. Reciprocity theroem for the calculation of average scattering properties of agglomerated particles. *Appl Opt* 2000;39:5827–33.
- [21] Xu Y-L, Gustafson BA. Orientation-averaged radiative properties of an arbitrary configuration of scatterers. *JQSRT* 2003;79-80:1121–37.
- [22] Lu N, Sorensen CM. Depolarized light scattering from fractal soot aggregates. *Phys Rev E* 1994;50:3109–15.
- [23] Seeley G, Keyes T, Ohtsuki T. Higher-order fractal geometry; application to multiple light scattering. *Phys Rev Lett* 1988;60:290–3.
- [24] Farias TL, Carvalho MG, K''oyl''u ''U''O, Faeth GM. Computational evaluation of approximate rayleigh-debye-gans/fractal-aggregate theory for the absorption and scattering properties of soot. *J Heat Transfer* 1995;117:152–9.
- [25] Saltiel C, Manickavasagam S, Chen Q, Schadler LS, Siegel RW, Mengüç MP. Identification of the dispersion behaviour of surface treated nanoscale powders. *J Nanopart Res* 2004;6:35–46.
- [26] di Stasio S. Feasability of an optical experimental method for the sizing of primary spherules in sub-micron agglomerates by polarized light scattering. *Appl Phys B* 2000;70:635–43.
- [27] di Stasio S. Observation of restructuring of nanoparticle soot aggregates in a diffusion flame by static light scattering. *J Aerosol Sci* 2001;32:509–24.

- [28] di Stasio S. Experiments on depolarized optical scattering to sense in situ the onset of early agglomeration between nano-size soot particles. *JQSRT* 2002;73:423–32.
- [29] di Stasio S, Massoli P. A dissymmetry ratio optical technique as applied to scattering pattern recognition of differently shaped soot aggregates. *Combust Sci Technol* 1997;124:219–99.
- [30] di Stasio S, Massoli P. A dissymmetry ratio optical technique as applied to scattering pattern recognition of differently shaped soot aggregates. *Part Part Syst Charact* 1998;15:90–9.
- [31] di Stasio S, Konstandopoulos AG, Kostoglou M. Cluster–cluster aggregation kinetics and primary particle growth of soot nanoparticles in flame by light scattering and numerical simulations. *J Colloid Interf Sci* 2002;247:33–46.
- [32] S. di Stasio, Recent research developments in applied physics, vol. 6, 2004.
- [33] Smyth KC, Shaddix CR. The elusive history of $m = 1.57 - 0.56i$ for the refractive index of soot. *Combust Flame* 1996;107:314–20.
- [34] Dalzell WH, Sarofim HF. Optical constants of soot their appl. to heat-flux calculations. *J Heat Transfer* 1969;36:100–4.
- [35] Brasil AM, Farias TL, Carvalho MG. Evaluation of the fractal properties of cluster–cluster aggregates. *J Aerosol Sci* 2000;33:441–54.